RSC Advances

PAPER

View Article Online
View Journal | View Issue

Cite this: *RSC Adv.*, 2016, **6**, 107871

Structural distortion and electronic states of Rb doped WO_3 by X-ray absorption spectroscopy

Y. C. Wang,[ab] C. H. Hsu,[a] Y. Y. Hsu,[cd] C. C. Chang,[a] C. L. Dong,[de] T. S. Chan,[d] Krishna Kumar,[f] H. L. Liu,[b] C. L. Chen*[ad] and M. K. Wu[a]

Received 31st August 2016
Accepted 5th November 2016

DOI: 10.1039/c6ra21777j

www.rsc.org/advances

Rubidium tungsten bronzes (Rb_xWO_3) have recently attracted much attention due to their intriguing phenomena, such as complex structural phase transitions, strong electron–phonon coupling, and superconducting properties. This study investigates the local atomic and electronic structures of Rb_xWO_3 ($0.17 \leq x \leq 0.33$). X-ray powder diffraction patterns showed a hexagonal tungsten bronze (HTB) phase. X-ray absorption spectra (XAS) at the W L_3-edge and Rb K-edge of Rb_xWO_3 were carried out. The XAS analysis indicated a local distorted WO_6 octahedron which leads to a splitting of e_g and t_{2g} energy states in the tungsten 5d orbital and this splitting of energy levels exhibited an asymmetrical behavior at $x = 0.23$ and 0.27. Overall analysis revealed a distortion of local atomic structure of the WO_6 octahedra by rubidium doping, leading to the modification of the electronic structures of e_g and t_{2g} states in the tungsten 5d orbital, thereby accounting for the property changes in CDW formation and superconducting transition temperature of these materials.

Introduction

There have been tremendous advancements both experimentally and theoretically in superconductivity research in the past 30 years, since the discovery of high temperature superconducting cuprates in 1986. One most notable outcome of these efforts is the discovery of many new superconducting materials with a wide range of crystal structures and chemical compositions. Among the non-cuprate new superconductors discovered, Fe-based superconductors have become the focus of scientific investigations since their discovery in 2008. On the other hand, the physical properties of transition metal oxides have also been studied for decades. Their electrical properties are strongly affected by the surrounding lattice. For instance, in the case of WO_3, the anisotropic-shaped d-orbital electrons in tungsten interact differently with p-orbital electrons in oxygen.[1–4] This effect induces many unconventional behaviors, such as metal–insulator transition, magnetic ordering, *etc.* in materials like tungsten bronze (A_xWO_3), where A refers to an alkali or alkaline metal (Na, K, Rb, and Cs).[5–12] Rubidium doped tungsten bronze shows superconductivity below 6 K and the superconducting transition temperature (T_c) depends on Rb doping.[10] The transport properties of these materials showed interesting features such as an asymmetrical behavior for T_c dependence on Rb(x) doping. Stanley *et al.*, observed a T_c of ~5 K at $x = 0.17$ Rb concentration and a subsequent decrease to ~2 K at $x = 0.23$. However, no clear trend could be observed although a slight increase in T_c from 2 K at $0.26 < x < 0.33$ was reported and suggested a concentration dependent phase transition near $x = 0.25$ where the material did not show any sign of superconductivity.[10] The origin of how Rb varies the T_c and crystal structure is still unclear. The T_c suppression of tungsten bronze by doping causes a suppression of superconductivity and exhibits distinct physical properties.[10–14] Further, in Rb doped system, a metal–insulator transition at around 250 K along c axis was observed from resistivity measurements and has strong correlation with superconductivity.[10–15] The origin of superconductivity in Rb_xWO_3 was first explained by Sato *et al.* from neutron scattering experiments.[12,13] They proposed the low frequency vibration of rubidium ion in hexagonal channels (h-WO_3) as Einstein type phonon modes, which has substantial correlation to the electron–phonon coupling in superconductivity in addition to the highly mobile Rb ions in the hexagonal cage along c direction. The Einstein type phonon mode was also observed by Sagar *et al.* in KWO_3 from Raman scattering experiments.[8] They suggested that the metal–insulator transition in KWO_3 was caused by a competition between the lattice structural disorder and charge ordering in the WO_6 octahedron, which might have induced a weak charge density wave (CDW) ground state especially at low temperatures. Although some earlier reports prevail, a detailed investigation on the lattice

[a]*Institute of Physics, Academia Sinica, Nankang, Taipei, Taiwan. E-mail: chen.cl@nsrrc.org.tw*

[b]*Department of Physics, National Taiwan Normal University, Taipei, Taiwan*

[c]*Program for Science and Technology of Accelerator Light Source, National Chiao Tung University, Hsinchu, Taiwan*

[d]*National Synchrotron Radiation Research Center, Hsinchu, Taiwan*

[e]*Department of Physics, Tamkang University, New Taipei city, Taiwan*

[f]*Department of General Studies, Physics Division, Jubail Industrial College (JIC), Jubail Industrial City 31961, Kingdom of Saudi Arabia*

structural disorder and charge ordering in the WO_6 octahedron in hexagonal tungsten bronze (HTB) using advanced characterization tools is worthwhile to unravel the distinct superconductivity behavior exhibited by these type of materials. This is because in simple BCS theory one would expect T_c to be a monotonic increasing function of x, assuming a constant electron–phonon interaction. Earlier, studies have been carried out on the electron–phonon interactions in hexagonal alkali tungsten bronze.[8–15] The variation of T_c with Rb doping in tungsten bronze is discussed on the basis of the CDW instability along the c-direction which further depends on type of lattice phonons produced as the crystalline structure is distorted from octahedral symmetry due to doping.[10–15] The CDW instability is similar to the first order Jahn–Teller instability in molecules with incomplete degenerate levels and its formation reduces the carrier density at the Fermi level.[11] Further, the valence states of cations were suggested to have correlation with the exhibited physical properties. Consequently, the interaction between the W 5d-electrons and oxygen 2p-orbitals is of great importance as Rb ions are doped into the WO_6 octahedron. We envisage that the results from our paper would provide a rich ground for the detailed study into the mechanism responsible for these kind of non-cuprate superconductivity. Advanced technology arises from the understanding of fundamental science, and depends importantly on characterization tools for directly observing both physical and chemical properties. Without knowledge of the fundamental electronic and atomic structures of materials and the changes in their structures at various conditions, engineering these materials to widen their range of practical applications is tough. It is well known that X-ray absorption spectroscopy (XAS), including X-ray absorption near-edge spectroscopy (XANES) and extended X-ray absorption fine structure (EXAFS) is a powerful tool to study the local electronic and atomic structure of materials. In this work, XAS at W L_3-edge and Rb K-edge of Rb_xWO_3 at $x = 0.17$ to 0.33 revealed a striking correlation between the CDW formation and the extent of local structural distortion due to Rb doping. Based on analytic results, a schematic model is proposed for the structural distortion in the WO_6 octahedron with Rb doping, which is likely to dictate the T_c value of the system and hence the superconductivity with Rb doping. Many new exciting results that are of both fundamental and technological interest have emerged in a relatively short amount of time. This report elucidates a relevant but rarely utilized means of elucidating the fundamental electronic/atomic structure and lays a foundation for engineering better high T_c non-cuprate new superconductors.

Experiments

High quality tungsten bronze were grown by an optical zone-melting method, which is similar to the previous study on the growth by sealed quartz tubes as described by Stanley *et al.* and R. Brusetti *et al.*[10,14,15] The concentration were measured by the X-ray fluorescence spectrometer (ZSX Primus II, Rigaku, Japan) to describe the Rb content. The sample quality was characterized with X-ray powder diffraction using Phillips diffractometer. The magnetic properties were measured using a SQUID Magnetometer (Quantum Design make) and resistivity measurements were performed using a physical property measuring system (PPMS) of the same make; T_c was confirmed from both transport and magnetic measurements.[10] XAS at W L_3-edge and Rb K-edge were recorded at beamline BL01C and BL17C at National Synchrotron Radiation Research Center (NSRRC), Hsinchu, Taiwan. All spectra were normalized to unit step height in the absorption coefficient from well below to well above the edges. The standard metal foils and oxide powders of WO_3 were used for energy calibration.

Results and discussion

Fig. 1(a) presents the powder X-ray diffraction patterns of Rb_xWO_3 at various Rb doping concentrations (x from 0.17 to 0.33). The diffraction peaks are indexed according to the hexagonal structure with the space group $P6_3/mcm$ (JCPDS 34-0394). No diffraction peak from pure Rb metal is noticed within the detection limit. The main phase of tungsten oxide have been identified as h-WO_3. A small additional diffraction peak is observed in the low Rb content, at around 23°, when $x < 0.21$. It can be identified as intergrowth tungsten bronzes (ITB) phase, 3-ITB phase.[16] The h-WO_3 structure builds up by WO_6 octahedral, sharing their corner oxygen atoms with each other to form

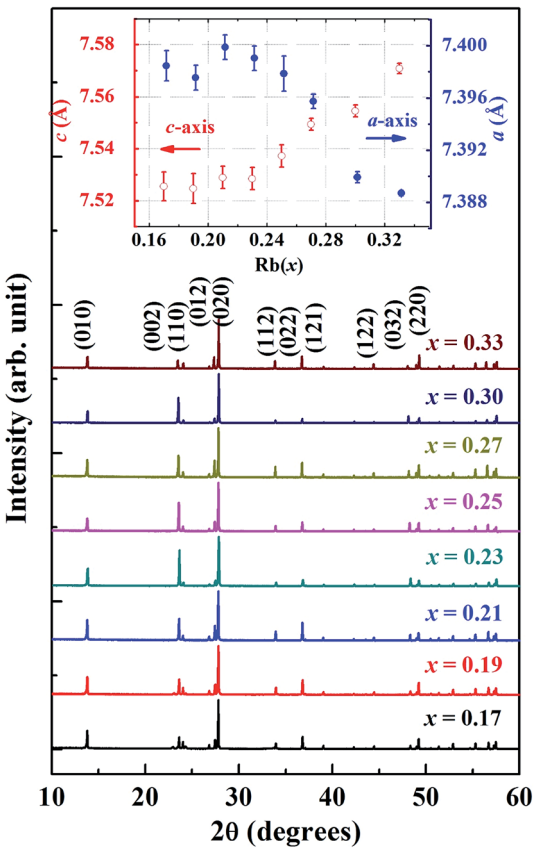

Fig. 1 X-ray diffraction pattern of Rb_xWO_3. Inset shows the lattice constant (a and c values marked in blue and red respectively) as a function of Rb doping(x).

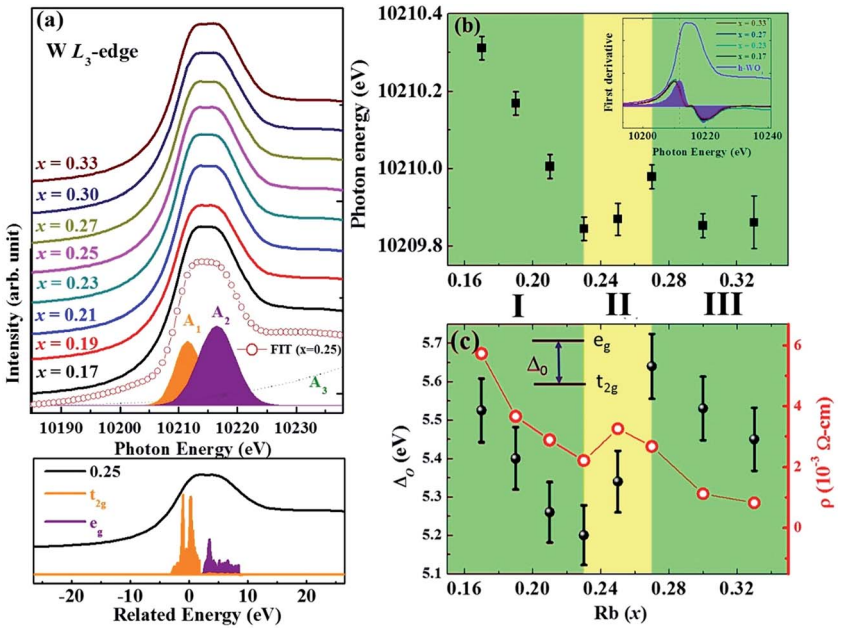

Fig. 2 (a) W L_3-edge XANES spectra of Rb_xWO_3. The DOS calculation and $x = 0.25$ spectra with the estimated t_{2g} and e_g states is shown in the bottom of figure. (b) The absorption edge position as a function of Rb doping, the edge of h-WO_3 is at 10 211.797 eV. Inset shows the first derivative W L_3-edge XANES spectra at various Rb doping. (c) The crystal field splitting energy (Δ_0, left black colored axis) and the measured resistivity (ρ, right red colored axis) as a function of different Rb doping.

a hexagonal tunnel along *c*-axis and the Rb ions are located in the hexagonal tunnels of the lattice. The radius of the tunnel is about 2 Å and the Rb ionic radius is 1.47 Å.[9,10] Therefore, Rb ions are free to occupy randomly in the tunnel site. A comparison with the undoped WO_3 show a shift in the diffraction peak position with Rb doping, denoting a change in lattice parameters. The lattice parameters *a* and *c* estimated at various Rb doping are plotted in the inset of the Fig. 1, which clearly shows a significant decrease and increase in *a* and *c*-parameters respectively, at $x > 0.23$. These variations in lattice parameters are likely to cause a distortion of WO_6 octahedron to different extents, though the crystallinity of the h-WO_3 appears to be same. Brusetti *et al.*, speculated a remodeling of WO_6 octahedra at low doping which make some associated phonons more active in the electron–phonon coupling.[14,15]

XANES provides information on the symmetry of the unoccupied electronic states. Fig. 2(a) presents W L_3-edge XANES spectra of Rb_xWO_3, *x* is ranged from 0.17 to 0.33. The strong resonance near the absorption edge in the energy region 10 190–10 225 eV is due to the excited electron transfer from W $2p_{3/2}$ to 5d unoccupied states with multiple excitations for hybridized W 5d–O 2p conduction band states.[17–20] XANES is sensitive to the local structural symmetry and to the influence of the bonding effect with oxygen ligands. The W L_3-edge spectra exhibit several features and are consistent with the h-WO_3 electronic structural calculations on crystal-field 10 D_q results of the O_h symmetries.[18] The figure shows two prominent features A_1 and A_2, which are attributed to the splitting of W 5d orbital into t_{2g} and e_g degenerate states, respectively, due to crystal field effect. To study the symmetry of W 5d electronic states, the decomposed $A_1(t_{2g})$ and $A_2(e_g)$ features are obtained by subtracting the arctangent (edge jump for step function) curve with best fitted Gaussian curves (absorption white line) (as shown in the bottom of Fig. 2(a)).[19,20] The fitted spectrum is consistent with the result from first principle calculation, as shown in the bottom of Fig. 2(a) which depicts a W L_3-edge XANES spectra of h-WO_3 and the corresponding density of states (DOS) t_{2g} and e_g orbitals.[18] The band-structure calculations were carried out in the scheme of generalized gradient approximation GGA with the on-site Coulomb interaction U taken into account,[18] *i.e.*, GGA+U calculations, are presented to interpret the XAS results. Fig. 2(a) shows that the line profiles of the spectra are nearly identical for Rb_xWO_3, irrespective of Rb

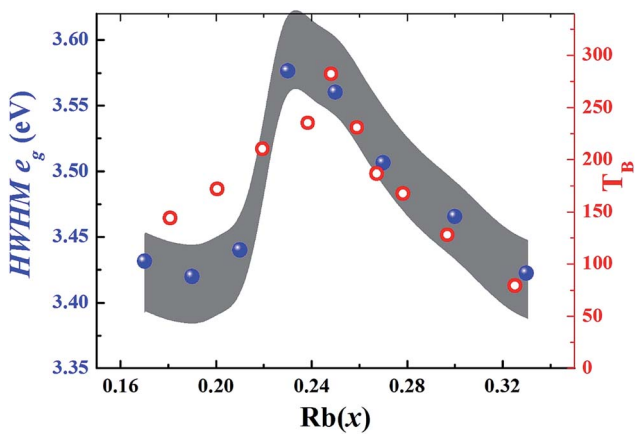

Fig. 3 The full width at half maximum (FWHM) values of e_g states (marked in blue) at various Rb doping. CDW onset temperature T_B as a function of *x* in Rb_xWO_3 is also shown (adapted from ref. 10).

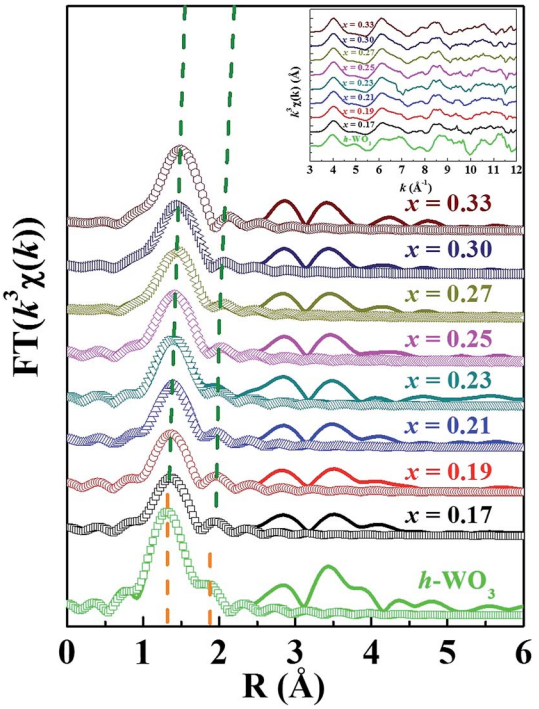

Fig. 4 EXAFS results (solid line) from the W L_3-edge. The FEFF fitting (open symbols) presents the WO_6 octahedral coordination. The inset shows the *k* space results.

doping and closely resemble that of h-WO_3. These findings are consistent with the XRD data where no major change was noticed in the hexagonal structure irrespective of Rb doping. Further, it is noticed that the integrated area of W L_3-edge for the Rb_xWO_3 almost matches with the h-WO_3 standard which means that the total unoccupied state of W 5d hole does not change when Rb is doped into WO_6 octahedra. This finding imply that the valence of W in all the Rb_xWO_3 samples is not altered and may therefore be confirmed as 6+. Fig. 2(b) presents the shift of W L_3-edge as a function of Rb doping which are obtained from first derivative W L_3-edge XANES spectra.[19,20] Inset of Fig. 2(b) shows W L_3-edge XANES first derivative spectra of Rb-doped WO_3 and reference h-WO_3. A shift of ~0.5 eV in the absorption edge between the $x = 0.17$ and 0.23 are observed (region I). A shift in the W L_3-edge XANES spectra of H_xWO_3 from that of pure W and h-WO_3 spectrum was reported earlier, which was due to the displacement of the electron density of W atoms.[17] The absorption edge shift in W L_3-edge XANES, especially at $x \leq 0.23$ may be attributed to a change in the energy gap, as suggested by Sato *et al.*[12] They suggested an alteration in the energy gap and Fermi level position in the electronic structure of tungsten, with a maximum around $x = 0.25$. Unlike the region I in which the energy of absorption edge position is monotonically decreased with an increase in Rb concentration, the absorption edge shifts to high energy as $x = 0.23$ increases to 0.27 in region II. Indeed to fully understand the structure of Rb_xWO_3, its phase transition and the lattice distortions in WO_6 octahedra with doping, it is necessary to have a knowledge on how the structural models were built. K. S. Lee *et al.*[11] performed the electronic band structure calculations on Rb_xWO_3 and presented a detailed structural model to explain the metal–semiconductor–metal phase transition. Further, P. Krüger *et al.*,[18] carried out a density functional theory study on pure and potassium doped tungsten trioxide which has a similar structure to Rb_xWO_3 and estimated the DOS. In Fig. 2(b), three distinct regions (I, II, III) with different colors represent the phase transition. The green and yellow regions represent the metal and semiconductor phases of Rb_xWO_3 respectively. From a band structure calculation,[18] the Fermi level (E_F) of WO_3 can be tailored by introduction of Rb and subsequent lattice structural distortion. Thus the lower part of conduction band which is composed of W 5d-t_{2g} band and 5d-e_g band is critical. The W 5d-t_{2g} band (unoccupied states above E_F) exhibit mainly electron–orbital interaction in 5d characters. Above results suggest that presence of Rb can cause the energy shift of W 5d states and thus modify the DOS around the Fermi level. BCS theory suggests that superconducting state is strongly correlated to the electron–phonon interactions. T_c increases with an increase in the electron–phonon coupling. A reduced electron–phonon interaction and thus a decrease in T_c at $x = 0.25$ was reported earlier by K. S. Lee *et al.*[11] As x decreases ($x < 0.33$) in Rb_xWO_3, cation vacant sites increases and are randomly distributed creating a random potential for conducting electrons. However, this is expected to suppress the superconductivity. Hence, disappearance of superconductivity at $x = 0.25$ is likely to be due to CDW formation associated with the 1D Fermi surface which removes lattice phonons that contribute to superconductivity. Their calculations also showed the presence of 1D as well as 3D Fermi surfaces in the system.[11] In general, more doping of Rb ions increase the stiffness of the WO_3 lattice which reduces the chance of CDW formation, whereas the electronic instability favors. Briefly, the CDW formation depends on the interplay of lattice stiffness and the electronic instability.[11] It is

Table 1 Estimated fitting parameters for the first and second shell from Rb_xWO_3 and h-WO_3 EXAFS spectra. *N* stands for the oxygen coordination number, σ^2 is the Debye–Waller factor, and *R* is the length of W–O bonding

Sample	Shell	*N*	σ^2	*R* (Å)
h-WO_3	1	4	0.005	1.7714 (±0.003)
	2	2	0.004	2.0456 (±0.005)
$Rb_{0.17}WO_3$	1	4.009	0.007	1.8303 (±0.010)
	2	1.982	0.005	2.0123 (±0.001)
$Rb_{0.19}WO_3$	1	4.009	0.006	1.8403 (±0.002)
	2	1.973	0.004	2.0172 (±0.006)
$Rb_{0.21}WO_3$	1	3.977	0.006	1.8405 (±0.003)
	2	1.984	0.006	2.0017 (±0.009)
$Rb_{0.23}WO_3$	1	3.782	0.004	1.8451 (±0.010)
	2	2.158	0.004	1.9854 (±0.006)
$Rb_{0.25}WO_3$	1	4.442	0.007	1.8559 (±0.008)
	2	1.479	0.007	2.0423 (±0.005)
$Rb_{0.27}WO_3$	1	4.543	0.009	1.8622 (±0.002)
	2	1.367	0.009	2.0700 (±0.008)
$Rb_{0.30}WO_3$	1	4.7	0.009	1.8779 (±0.003)
	2	1.2	0.009	2.1399 (±0.007)
$Rb_{0.33}WO_3$	1	4.824	0.008	1.8888 (±0.006)
	2	1.002	0.005	2.0159 (±0.008)

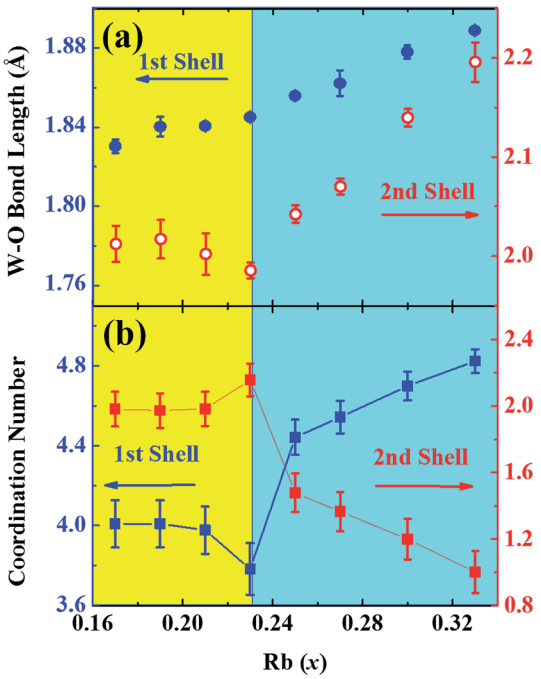

Fig. 5 (a) The W–O bond length in first (blue) and second (red) shell, (b) is the oxygen coordination number in first and second shell.

worth to recall that an interesting behavior of Rb_xWO_3 type materials is their composition dependent resistivity anomaly that has strong correlation with CDW formation. The superconductivity behavior of these materials is also correlated to the CDW onset temperature T_B at which resistivity anomaly occurs (an anomalous hump in the resistivity).[8,10,11] A few reports also indicated an electron–hole correlations in A_xWO_3 due to W ions at distorted lattice structure which may influence the electronic transport behavior.[21,22]

Fig. 2(c) depicts the Δ_0 ($\Delta_0 = A_2(e_g) - A_1(t_{2g}) = 10\ D_q$), estimated by the O_h crystal field theory, as a function of Rb doping. The t_{2g}–e_g splitting energy levels in the 5d with Rb doping suggests an instability and distortion of O_h symmetry. The d orbital splitting directly reflects the energy gap.[20] The result demonstrates that Δ_0 is minimum at $x = 0.23$ and maximum at $x = 0.27$. Interestingly, the room temperature resistivity (ρ) of Rb_xWO_3 at various doping levels shows a similar behavior to Δ_0 (Fig. 2(c)). The resistivity gradually decreases from $x = 0.17$ to 0.23, exactly in the same trend as T_c decreases with x and recall that Rb_xWO_3 exhibit metallic properties in this region. Thus, it can be deduced that both the effect of lattice structure modulation and electronic-orbital overlapping variations with doping lead to the state of semiconductor behavior along with no sign of superconductivity in the range $0.23 < x < 0.27$. At the metal–semiconductor–metal phase transition region in Rb_xWO_3, the instability in the local structure as discussed above can make changes in the W 5d band structure and the position of E_F. CDW can cause an electronic instability, and it is strongly correlated to the variation in the crystal structure. The W 5d orbital symmetry is strongly correlated to the crystal lattice and corner-sharing atoms in WO_6 octahedron. Thus, the values of full width at half maximum (FWHM) of e_g states (marked in blue) are estimated and plotted as a function of Rb doping in Fig. 3. A maximum at $x = 0.23$ is observed in Fig. 3. As the e_g (d_{z^2} and $d_{x^2-y^2}$) orbitals point directly to the corners of WO_6 octahedron, the variation in FWHM e_g unoccupied states with Rb doping is likely to cause a distortion in the octahedron. The CDW onset temperature T_B as a function of x in Rb_xWO_3 (adapted from ref. 10) is also included in Fig. 3 for comparison. Interestingly, the variation in T_B show a maximum near $x = 0.25$. The similar trend in the variation of FWHM e_g and T_B again suggest that the Rb doping changes the structural ordering and modifies the local structure symmetry of WO_3.[11,12] Therefore, it is essential to investigate the local atomic structure of Rb_xWO_3 using EXAFS.

Fig. 4 shows Fourier transform (FT) of EXAFS $k^3\chi$ data at the W L_3-edge from $k = 3$ to 11 $Å^{-1}$ (inset) for Rb_xWO_3 at various Rb doping and the reference h-WO_3. For all samples, radial distribution of FT spectra are similar to each other. The FT profiles in real (R)-space provide direct evidence on the changes in the W–O bond length, coordination number, and Debye–Waller factor (σ^2).[23] The first two main peaks near 1.38 and 1.85 Å correspond to the first (W–O1), nearest neighbor, and second (W–O2), next nearest neighbor, shells/bond length in the WO_6 octahedron, respectively.[19,20,24] The O1 and O2 corresponds to the oxygen atom in the equatorial and axial positions in the octahedron, respectively. The EXAFS curves are fitted by FEFF analysis using ARTEMIS program[23] (open symbols in Fig. 4) and the results are presented in Table 1. The spectra shows a best fitting within the limits of 0.5 Å and 2.3 Å. Fig. 5(a) shows the variation of W–O bond length in the first and second shell in WO_6 octahedron (from Fig. 4) as a function of Rb doping. The figure demonstrates that the W–O1 bond length (blue) increases from 1.83 Å at $x = 0.17$ to 1.888 Å at $x = 0.33$, the error in bond length is less than ±0.01. In contrast, the W–O2 bond length (red) slightly decreases with Rb doping initially (*i.e.* $x = 0.17$ to 0.23) and then increases. The W–O bond length variation (Fig. 5(a)), especially asymmetrical shift of the second shell near $x = 0.23$, imply that the structural symmetry of WO_6 (O_h) octahedron has distorted keeping the hexagonal structure, which is consistent with the XRD analysis. The FWHM of W 5d-e_g orbital exhibits a maximum value at $x = 0.23$ (Fig. 3). The increase in W–O bond length with Rb doping is attributed to the increased occupation of comparatively large atomic radius Rb compared to W. This probably create an increased disorder in the WO_6 octahedron, with a local lattice distortion that may lead to changes in the lattice phonon behavior. Fig. 5(b) compares the

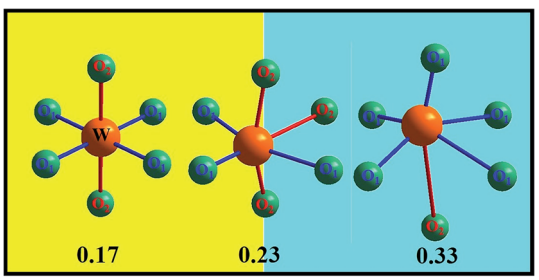

Fig. 6 The model of distortion in octahedral.

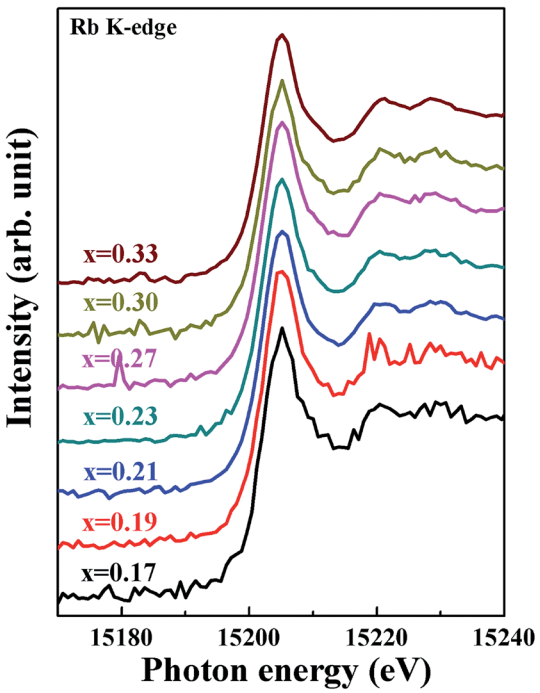

Fig. 7 Rb K-edge XANES spectra of Rb_xWO_3.

coordination number (CN) of first and second shells as a function of Rb doping. The result indicates a discontinued change of CN at $x = 0.23$ for both the O1 (blue) and O2 (red) cases. The CN in the first shell indicates a substantial decrease (increase) at $x \leq 0.23$ ($x \geq 0.23$). In contrast, the second shell demonstrate an opposite trend. These changes in the CN suggest an off center effect in the octahedron as predicted by earlier electronic structure calculation.[6,25] In order to get an insight into the local structural modification caused by Rb doping and the nature of distortion in WO_6 octahedral symmetry, a schematic model of distortion duly taking account of W–O1 and W–O2 variation is presented in Fig. 6. The W–O bond length and CN estimated from EXAFS analysis are also considered. Analytic results from Fig. 5 and 6 infer that at low Rb doping, though the WO_6 octahedron does not exhibit a major distortion, the W–O bond length along *z*-axis increases. As the Rb doping gradually increases to 0.23, it appears that the position of central W ions is modulated and shifted in the *xy*-plane (equatorial) of octahedron. In this region, CN slightly increases in second shell (W–O2) and a corresponding decrease is observed in the first shell (W–O1). Further increase in Rb doping ($x > 0.23$) results the structure (octahedron) extend along *z*-axis at one side that lead to an increase in CN of W–O1 and a corresponding decrease in W–O2. To sum up, Rb doping caused a local structure distortion and the tungsten ions off center in the WO_6 octahedron. The electron–phonon coupling mechanism in quasi-1-D lattice structure is contributed by vibration of Einstein-like phonon modes.[10–15] Hence, the change of local electronic structure and distortion of local atomic structure of the WO_6 octahedron, revealed by XANES and EXAFS, modify the electron–phonon coupling in Rb_xWO_3 and generate an Einstein-like phonon mode vibration. This alteration in the phonon mode vibration accounts for the superconducting transition temperature and CDW formation in Rb_xWO_3. Recall that the W L_3-edges XANES indicate a variation in the W5d-orbital electronic states due to the t_{2g}–e_g splitting of energy levels by the ligand fields of the surrounding oxygen atoms and an associated distortion in the local structure symmetry by Rb doping. Further, it is worth to point out that our Rb K-edge XANES of Rb_xWO_3, as shown in Fig. 7, does not show any change in the Rb valence with Rb doping which is consistent with other studies on hexagonal alkali tungsten bronzes A_xWO_3 (A = K, Rb and Cs) that A^+ cations are occupied at the tunnel of hexagonal lattices. Finally, this study indicate an off center shift for tungsten ions in WO_6 octahedral symmetry and an associated change in phonon mode of vibration. Analytic result from XAS evidences the changes in W 5d electronic states and the local structural distortion cause the suppression of superconductivity and the phase transition in Rb_xWO_3.

Conclusion

We investigated the effects of Rb doping in WO_3 using XAS techniques. The local electronic and atomic structures, as well as their correlation to the superconducting properties are discussed. XAS results corroborate with the CDW formation in Rb_xWO_3 likely due to changes in electro–phonon interaction in the octahedral symmetry of WO_6 octahedron. Spectroscopic result indicates a shift in the Fermi level with Rb doping and a change in coordination number, and subsequent variation in electron–phonon coupling. An increase in the lattice phonon interaction is originated from the local structure distortion as a result of Rb doping. Combined XANES and EXAFS analyses reveals the WO_3 in Rb_xWO_3 has regular hexagonal phase with a distortion in the O_h coordination structure and an off center at $x \leq 0.23$. These findings suggest a change in phonon scattering which may be correlated with the distinct superconductivity behavior in Rb_xWO_3. Our study suggests the possibility of tuning the physical properties of these type of materials by correlating their electronic/atomic structures and CDW formation. Further, an enhanced knowledge concerning the behavior and better understanding the mechanism of superconductivity in Rb_xWO_3 and related compounds is very important for potential to find new high T_c non-cuprate superconductors.

Acknowledgements

This work is supported by the Ministry of Science and Technology (MOST) (formerly the National Science Council (NSC)) of Taiwan, under contracts no. MOST 102-2112-M-001-004-MY3. The authors are grateful to Prof. H. C. Hsueh for band structure calculation and NSRRC for providing beamtime and beamline support.

References

1 E. Dagotto, *Rev. Mod. Phys.*, 1994, **66**, 763.
2 J. Orenstein and A. J. Millis, *Science*, 2000, **288**, 468.
3 E. Canadell and M. H. Whangbo, *Chem. Rev.*, 1991, **91**, 965.

4 S. S. Zumdahl and S. A. Zumdahl, *Chemistry*, Houghton Mifflin, 7th edn, 2007.
5 B. W. Brown and E. Banks, *J. Am. Chem. Soc.*, 1954, **76**, 963.
6 F. Corà, M. G. Stachiotti and C. R. A. Catlow, *J. Phys. Chem. B*, 1997, **101**, 3945–3952.
7 M. R. Skokan, W. G. Moulton and R. C. Morris, *Phys. Rev. B: Condens. Matter Mater. Phys.*, 1979, **20**, 3670.
8 D. M. Sagar, D. Fausti, S. van Smaalen and P. H. M. van Loosdrecht, *Phys. Rev. B: Condens. Matter Mater. Phys.*, 2010, **81**, 045124.
9 L. H. Cadwell, R. C. Morris and W. G. Moulton, *Phys. Rev. B: Condens. Matter Mater. Phys.*, 1981, **23**, 2219.
10 R. K. Stanley, R. C. Morris and W. G. Moulton, *Phys. Rev. B: Condens. Matter Mater. Phys.*, 1979, **20**, 1903.
11 K.-S. Lee, D.-K. Seo and M.-H. Whangbo, *J. Am. Chem. Soc.*, 1997, **119**(17), 4043–4049.
12 M. Sato, B. H. Grier, H. F. Fujishita, S. Hoshino and A. R. Moodenbaugh, *J. Phys. C: Solid State Phys.*, 1983, **16**, 5217–5232.
13 M. Sato, B. H. Grier, G. Shirane and H. Fujishita, *Phys. Rev. B: Condens. Matter Mater. Phys.*, 1982, **25**, 501.
14 R. Brusetti, P. Bordet, J. Bossy, H. Schober and S. Eibl, *Phys. Rev. B: Condens. Matter Mater. Phys.*, 2007, **76**, 174511.
15 R. Brusetti, P. Haen and J. Marcus, *Phys. Rev. B: Condens. Matter Mater. Phys.*, 2002, **65**, 144528.
16 C. Grenthe, M. Sundberg, V. P. Filonenko and I. P. Zibrov, *J. Solid State Chem.*, 2000, **154**, 466–475.
17 O. Y. Khyzhun, Y. M. Solonin and V. D. Dobrovolsky, *J. Alloys Compd.*, 2001, **320**, 1–6.
18 P. Krüger, I. Koutiri and S. Bourgeois, *Phys. Rev. B: Condens. Matter Mater. Phys.*, 2012, **86**, 224102.
19 (*a*) M. V. Limaye, J. S. Chen, S. B. Singh, Y. C. Shao, Y. F. Wang, C. W. Pao, H. M. Tsai, J. F. Lee, H. J. Lin, J. W. Chiou, M. C. Yang, W. T. Wu, J. S. Chen, J. J. Wu, M. H. Tsai and W. F. Pong, *RSC Adv.*, 2014, **4**, 5036; (*b*) J. Purans, A. Kuzmin, P. Parent and C. Laffone, *Ionics*, 1998, **4**, 101–105.
20 (*a*) S. Yamazoe, Y. Hitomi, T. Shishido and T. Tanaka, *J. Phys. Chem. C*, 2008, **112**, 6869–6879; (*b*) C. L. Chen, C. L. Dong, S. M. Rao, G. Chern, M. C. Chen, M. K. Wu and C. L. Chang, *J. Phys.: Condens. Matter*, 2008, **20**, 255236.
21 A. M. Gabovich, A. I. Voitenko, J. F. Annett and M. Ausloos, *Supercond. Sci. Technol.*, 2001, **14**, R1–R27.
22 S. K. Deb, *Sol. Energy Mater. Sol. Cells*, 2008, **92**, 245–258.
23 B. Ravel and M. Newville, *J. Synchrotron Radiat.*, 2005, **12**, 537–541.
24 A. Kuzmin and J. Purans, *J. Phys.: Condens. Matter*, 1993, **5**, 2333–2340.
25 A. D. Walkingshaw, N. A. Spaldin and E. Artacho, *Phys. Rev. B: Condens. Matter Mater. Phys.*, 2004, **70**, 165110.